

## Article

# Multichromic Behavior of Liquid Crystalline Composite Polymeric Films

Mizuho Kondo <sup>1,\*</sup>, Satoka Yanai <sup>1</sup>, Syouma Shirata <sup>1</sup>, Takeshi Kakibe <sup>2</sup>, Jun-ichi Nishida <sup>1</sup>  
and Nobuhiro Kawatsuki <sup>1</sup>

<sup>1</sup> Department of Applied Chemistry, Graduate School of Engineering, University of Hyogo, 2167 Shosha, Himeji 671-2280, Japan; et21c002@steng.u-hyogo.ac.jp (S.Y.); r4.sshirata@gmail.com (S.S.); jnishida@eng.u-hyogo.ac.jp (J.-i.N.); kawatuki@eng.u-hyogo.ac.jp (N.K.)

<sup>2</sup> Department of Chemical Engineering, Graduate School of Engineering, University of Hyogo, 2167 Shosha, Himeji 671-2280, Japan; kakibet@eng.u-hyogo.ac.jp

\* Correspondence: mizuho-k@eng.u-hyogo.ac.jp; Tel.: +81-79-267-4014

**Abstract:** In this study, we describe the synthesis of a cholesterol-linked cyanostilbazole salt dye and the tuning of its luminescence by physical stimuli such as electricity and grinding. The dyes exhibited liquid-crystalline properties at temperatures above 170 °C. Some of the solutions were transformed into orange luminescent gels upon the addition of poor solvents. When the solvent was evaporated, the resulting solid xerogel exhibited mechanochromism, its color changed, and its luminescent color changed from orange to red. Furthermore, we investigated the construction of functional gels (mechanochromic gels) that can respond to two stimuli, damage detection by abrasive responsiveness, and electrical response using ionic liquid complexes of polymers as dispersing media. This study provides a new strategy for tuning and switching luminescence using non-chemical stimuli in a single-component system using aggregation.

**Keywords:** mechanofluorochromic dye; liquid crystal; gel; electrochromism



**Citation:** Kondo, M.; Yanai, S.; Shirata, S.; Kakibe, T.; Nishida, J.-i.; Kawatsuki, N. Multichromic Behavior of Liquid Crystalline Composite Polymeric Films. *Crystals* **2023**, *13*, 786. <https://doi.org/10.3390/cryst13050786>

Academic Editor: Francesco Simoni

Received: 28 April 2023

Revised: 3 May 2023

Accepted: 4 May 2023

Published: 9 May 2023



**Copyright:** © 2023 by the authors. Licensee MDPI, Basel, Switzerland. This article is an open access article distributed under the terms and conditions of the Creative Commons Attribution (CC BY) license (<https://creativecommons.org/licenses/by/4.0/>).

## 1. Introduction

Low-molecular-weight gels are materials with a continuous structure of macroscopic dimensions composed of a low concentration of gelator and solvent, and exhibit rheological behavior similar to that of solids. Gels formed by low-molecular-weight gelators have been put to practical use as aggregating agents, taking advantage of their ability to switch between flowable sol and solid-state gel upon exposure to external stimuli. They are also expected to be applied in a wide range of fields, such as drug delivery [1], sensors, and self-healing materials [2], and are being intensively studied. Recently, aggregation-induced emission (AIE) gelators, in which a luminescent moiety is introduced into low-molecular-weight gelators and the luminescence behavior changes significantly during the gel-to-sol and sol-to-gel phase transitions, have attracted attention from both theoretical and practical perspectives [3,4]. AIE gels have the potential to be excellent stimulus-responsive luminescent materials because their luminescence behavior changes in tandem with the aggregation and disassembly of supramolecular networks induced by various external stimuli. In particular, the mechano-responsive property, in which the luminescence behavior is changed by grinding, allows macroscopic mechanical stimuli to affect the optical properties of molecules and is expected to be applied to displacement and force sensors with excellent spatial resolution [5,6]. In recent years, many mechanochromic gels utilizing the intermolecular interactions of chitosan [7] and cholesterol [4], as well as mechanosensitive gels utilizing the cholesteric phase of liquid crystals [8] or the change in selective reflection of photonic crystals [9], have been reported. Small-molecule gels are generally produced by introducing long hydrophobic tails, such as cholesterol, alkyl chains, and alkoxy chains [10]. Many small-molecule organogelators have been investigated, among

which cholesterol has been extensively studied because of its ability to form stable gels through the synergistic effect of cooperative noncovalent bonding. However, cholesterol has a relatively rigid fused ring structure and can be used as a substituent for the development of liquid crystallinity. Furthermore, its gelation ability is expected to be enhanced without impairing liquid crystallinity. In dyes with the introduced liquid crystalline properties, functional mechanochromic (MC) behaviors can be realized, such as phase-dependent color control [11], multicolor luminescence [12,13], metastable color stability control [14], and orientation control [15,16]. Therefore, several research groups have investigated the combination of liquid crystalline properties and aggregation-induced luminescence. By introducing trans, a mesogen widely used to produce liquid crystals, more stable and aggregation-responsive polysynthetic dyes with excellent aggregation properties can be obtained. In a previous study, we synthesized a compound consisting of cholesterol, a gel-forming functional group, a cyanostilbene derivative, and a friability-responsive moiety linked to phenylacetylene. Cyanostilbene has a large dipole moment and twisted geometry along the central ethylene unit. It also tends to form stacked molecular sheets through multiple C–H—N and C–H—O hydrogen bonds. As these structures can be modified by external stimuli, they are frequently used as functional groups to express MC luminescence. Cyanostilbene derivatives also have donor–acceptor structures and tend to form antiparallel molecular pairs. The formation of molecular pairs leads to the formation of bifunctional cholesterol at the ends of the complexes, which are expected to form gels when linked one-dimensionally via intermolecular interactions [4,17]. In addition, we reported that the spin-coated film formed from the sol state exhibits a friability response, and that, by utilizing its liquid crystalline nature, it exhibits polarized luminescence when oriented parallel to the friability direction, enabling the recognition of the friability direction [18].

In the gel state, various functional liquids can be incorporated into the dispersing medium to form flexible functional composites and combining properties that are difficult to achieve using a single compound. In this study, we focused on ionic liquids (ILs) as a dispersing medium for functionalities because IL-composite polymer composite gels can be used as conductive materials and are expected to be applied for damage detection in conductive materials by providing a mechanical stimulus response. In addition, if the composite is electrically responsive (electrochromism (EC)) to ILs, functional gels (mechanochromic gels) that respond to both electrical and mechanical stimuli can be constructed. The addition of an EC response simplifies the control of coloration and responsiveness, enables flexible control of the physical properties, and can be applied to the detection of breakage and short circuiting of the electrolyte inside a battery. Although some studies have introduced MC dyes into films of conductors to enable the detection of external forces [19], no study has directly measured the load on a conductor. This is because the change in the MC dye manifests itself in crystalline and solid systems, whereas the electrical response manifests itself in solution systems, making it difficult to achieve compatibility. In this study, we attempted to achieve stimulus-responsiveness using the dye itself as a physical gel.

## 2. Results and Discussion

### 2.1. General Property of the Luminophore

Figure 1 shows the chemical structures of the luminophores used in this study. The synthesis and evaluation methods of the compounds are specifically described in the experimental section. The method of evaluation of the mechanoresponse is a method employed by many research groups. In a previous study, phenylacetylene was introduced at the end of the conjugated backbone; however, thiophene, which has a higher HOMO and smaller energy gap, was introduced in this study. Because cyanostyrobazole linked to thiophene exhibits a friability response even in the protonated state [17], friability is also expected in quaternized compounds. Therefore, to facilitate the expression of the electrical response, we changed the molecular end of the salt to a quaternized pyridine to make it a donor–acceptor salt. The optimized structures were determined using density functional

theory (DFT) calculations. Owing to limitations of the computational environment, the thiophene end was assumed to be a methyl group. Frontier orbital plots of the HOMO and LUMO of the optimized structure are shown in Figure 1b,c, respectively; the LUMO was mainly distributed in the acceptor of the cyanostilbene unit, while the HOMO was mainly located in the alkylthiophene unit. The energy levels of HOMO and LUMO are estimated to be 8.05 and 6.13 eV, respectively, with an energy gap between these levels of 1.92 eV. The energy-minimized structures exhibited twisted conformations and improved planarity of the cyanostilbazole moiety compared with the compounds before cholesterol introduction. These electronic structures were similar to those of the protonated cyanostyrobazole derivatives; cholesterol was predicted to be present in a bent conformation at right angles from the conjugated moiety. This is because, in the previous structure, cholesterol was linked to the quaternized cyanostyrobazole via a bromoacetate ester, whereas in the present structure, cholesterol was linked as a benzoate ester, and the linearity was reduced [18].

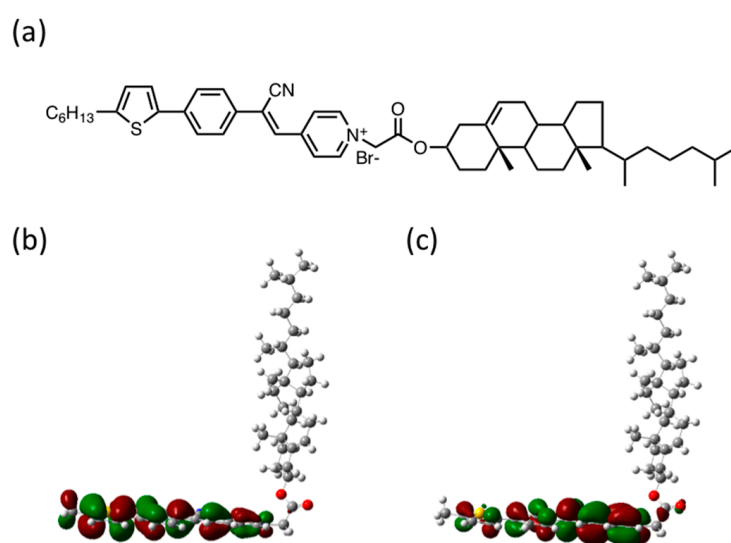


**Figure 1.** (a) Chemical structures and (b) HOMO and (c) LUMO of the luminophore used in this study. Red and green lobes represent positive and negative coefficients for molecular orbitals, respectively, and the size of each lobe is proportional to the magnitude of these coefficients.

These compounds were dissolved in various solvents, and their absorption and emission spectra were measured. The dyes were dissolved in common solvents, including toluene, tetrahydrofuran (THF), dimethyl sulfoxide (DMSO), and dichloromethane (DCM), which have increasing polarity in the order of toluene < THF < DCM < DMSO. An overview of the changes in the absorption spectra of the dyes dissolved in various solvents is shown in Figure 2a. The absorption shifted to longer wavelengths in more polar solvents. The differences in the luminescence behavior was more pronounced, with a significant red-shift in the photoluminescence (PL) spectral peak when dissolved in DMSO or DCM (Figure 2b).

The effect of the solvent polarity on the absorption spectrum was estimated using time-dependent TD-DFT calculations, and the results are shown in Figure 3. To simplify the calculations, a model compound with a methyl group at the styrobazole end, independent of the conjugation, was used. The  $\lambda_{\text{abs}}$  showed red shifts in the order DMSO < DCM < THF < toluene, which is opposite to the experimental results. All of these absorptions are HOMO-LUMO transitions. The reason for this discrepancy may be that the interaction with the solvent is not simple, and the contribution of Br as a counter ion was neglected in the calculations.

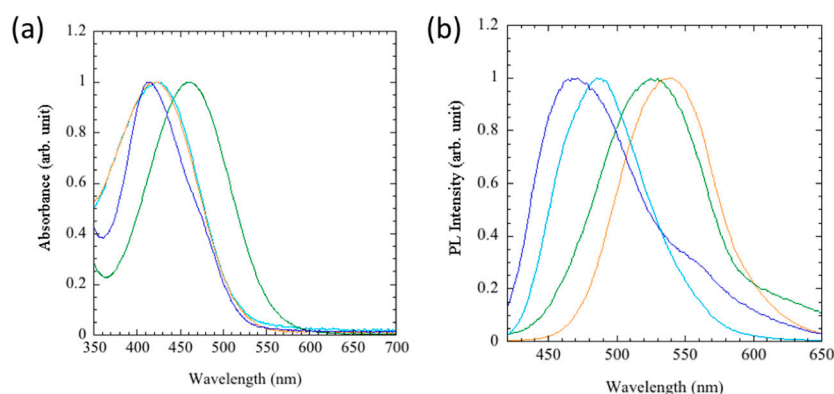


**Figure 2.** (a) Absorption and (b) photoluminescence (PL) spectra of the luminophore ( $1.0 \times 10^{-4}$  mol/L) dissolved in toluene, (blue) dichloromethane, (DCM, green) tetrahydrofuran (THF, blue), and dimethyl sulfoxide (DMSO, orange).

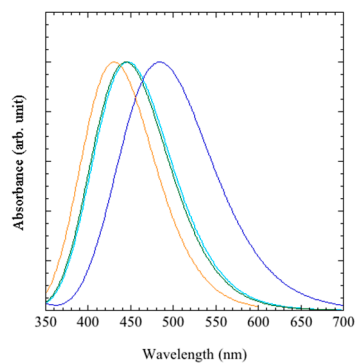


**Figure 3.** TD-DFT calculated absorption spectra of the luminophore dissolved in toluene (blue), DCM (green), THF (blue), and DMSO (orange).

## 2.2. Mechanoresponsive Behavior

The mechanical responses of the compound powders were evaluated. Figure 4a,b show the PL spectra and luminescence photographs before and after grinding, respectively. Figure 4c shows the change in the luminescence decay profile before and after grinding. Before grinding, the powder showed orange emission with a maximum emission wavelength of 637 nm and a fluorescence lifetime of 7.22 ns; after grinding in an agate mortar, the luminescence changed to red, with a maximum emission wavelength of 654 nm and a fluorescence lifetime of 7.44 ns, which did not change after additional grinding. The luminescence quantum yield changed from 1.8% to 1.7%. Unlike the previously gelled material, no long-lived luminescent components were detected, indicating excimer formation. Therefore, it can be inferred that excimer formation is not essential for a series of derivatives capable of gelation. In addition, the luminescence intensity did not change drastically with grinding, as in the case of the AIE-mediated dye, suggesting that the luminescence intensity changed via a mechanism different from that of AIE.

Scanning electron microscopy (SEM) observation of the powder was also performed on the powders. Fibrous structures were observed on the surface of the powder before grinding but not after grinding. Figure 5b shows the powder X-ray diffraction (XRD) results before and after the grinding of the powder. Some peaks were observed in the powder that disappeared after grinding. Compared to previous compounds, the peaks were broad and low in intensity. Therefore, the crystallinity was low and the powder was amorphous after grinding.

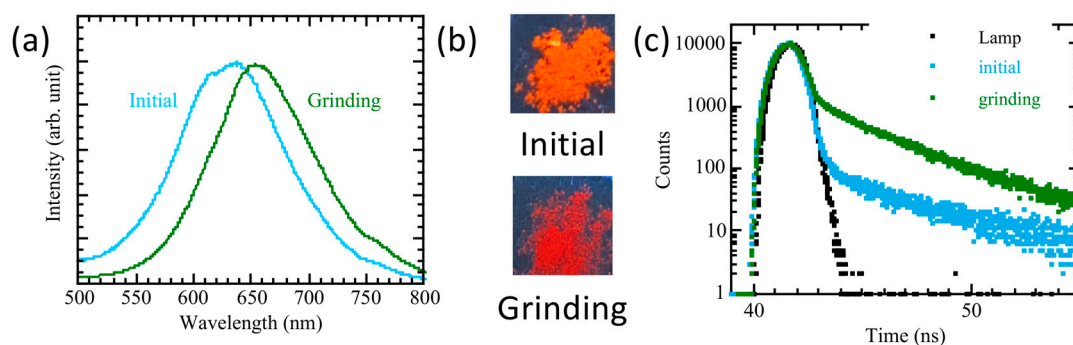


**Figure 4.** Change in (a) PL spectrum, (b) photoluminescent color, (c) and fluorescent decay profile of the luminophore before and after mechanical grinding.

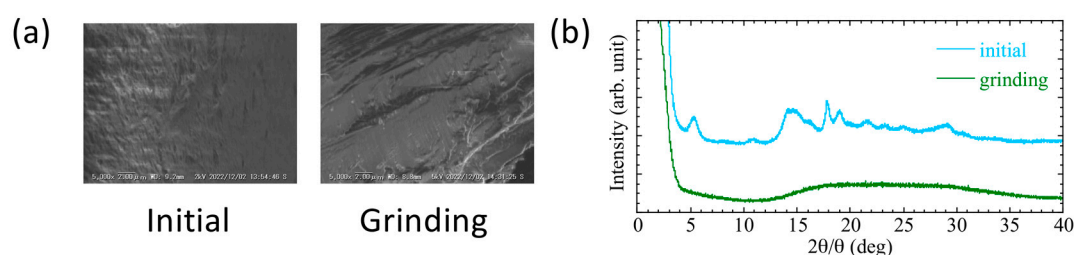


**Figure 5.** (a) Scanning electron microscopy images and (b) X-ray diffraction patterns before and after mechanical grinding. The scalebar in (a): 2 μm.

When the ground powder was heated, it formed a birefringent fluid phase and solidified when cooled to room temperature. The maximum emission wavelength remained unchanged at 637 nm during the series of operations, and the emission color did not change when the film was ground again. Differential scanning calorimetry (DSC) measurements of the dye showed that the slope of the thermogram changed at temperatures above 150 °C, suggesting that a change in the solid state was induced (Figure 6). The thermal properties disappeared in the second scan when the temperature was scanned up to 230 °C.

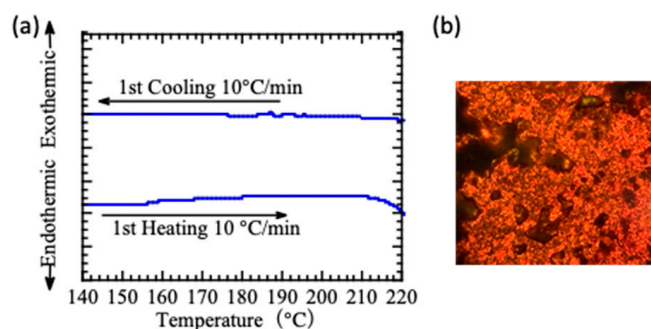


**Figure 6.** (a) Differential scanning calorimetry thermogram of the luminophore and (b) polarized optical microscopy image of the luminophore at 170 °C.

The fluid phase was presumed to be the liquid crystalline phase; however, unlike in a previous report, no optical structure derived from the cholesteric phase could be observed. This may be due to the fact that the cholesteric and rigid luminescent sites are not linearly connected and the liquid crystallinity is not stable.

While the compound did not gel in a single solvent, it gelled at a concentration of 14.3 g/L in a 6/1 (*v/v*) mixture of chloroform as a good solvent and hexane as a poor solvent (Figure 7). The gel showed fluidity when heated to 40 °C and reversible gelation when cooled to 4 °C.

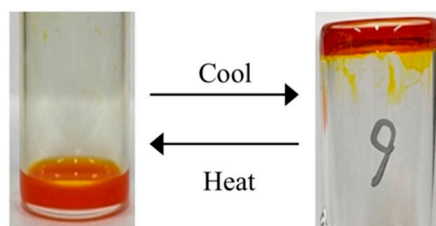


**Figure 7.** Inversion test of the luminophore dissolved in 6/1 (*v/v*) mixture of chloroform and hexane.

The material that changed color upon gelation retained its luminescent color even after the solvent was removed from the xerogel and exhibited a MC response. The changes in the PL spectra are shown in Figure 8a,b. The XRD patterns showed no diffraction peaks before and after grinding (Figure 8c). From SEM observations, the surface of the ground material showed a pattern similar to that of a fibrous structure before grinding but not after grinding (Figure 8d).

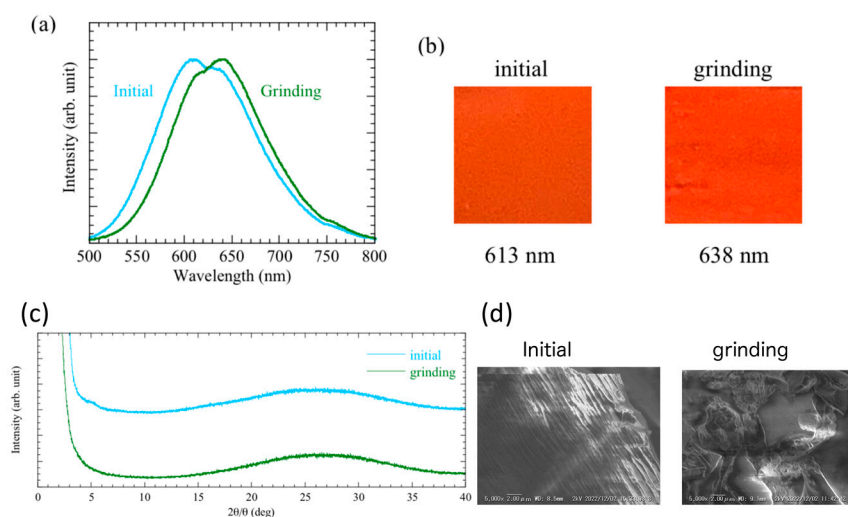


**Figure 8.** Mechano-induced changes in (a) PL spectrum, (b) photoluminescent color, (c) X-ray diffractogram, and (d) SEM image of the luminophore film prepared from the xerogel. The scalebar in (d): 2  $\mu\text{m}$ .

These results suggest that the color change is not due to the crystalline structure but rather to the one-dimensional structure of the solid and gel interiors and that less rigorous intermolecular interactions are responsible for the color change.

### 2.3. Electroresponsive Behavior

Materials that simultaneously exhibit AIE and EC have been reported by Sun et al. [20]. In addition, as mentioned in the introduction, some papers have reported that AIE-responsive materials connected to cholesterol exhibit MC. Taking these reports into consideration, we can expect to find cholesterol-based MC materials that exhibit EC. However, since EC is mainly a response in liquids and MC is mainly a response in solids, there have been no reports of systems in which EC and MC can be simultaneously expressed. On the other hand, there have been several reports of materials that exhibit EC in a gel composite [21–23], and therefore, it is expected that EC and MC can be expressed in the same system by utilizing a material that exhibits MC in a gel state. Accordingly, for the AIE system for cholesterol, we attempted EC with a material with a lower band gap based on the previous material.

The electrical response of the luminophore was evaluated by cyclic voltammetry measurements in DCM in the presence of tetrabutylammonium hexafluorophosphate ( $n\text{-Bu}_4\text{NClO}_4$ ) (0.1 M) with ferrocene  $\text{Fc}/\text{Fc}^+$  as an internal standard, showing only an

ambiguous one-electron oxidation at 0.18 V, indicating an irreversible electrical response (Figure 9). Based on these electrical responses, the HOMO and LUMO levels of the compound were estimated using the following equations:

$$\text{HOMO} = -(E_{\text{ox}} + 4.71)$$

$$\text{LUMO} = -(E_{\text{red}} + 4.71)$$

where  $E_{\text{ox}}$  and  $E_{\text{red}}$  are the oxidation and reduction voltages, respectively; the HOMO and LUMO are estimated to be  $-6.01$  and  $-3.91$  eV, respectively, and the band gap between these levels is 2.10 eV, which is close to the values estimated from the DFT calculations.

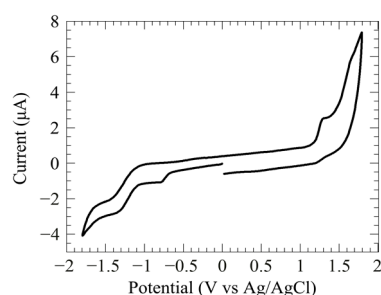


**Figure 9.** Cyclic voltammograms of the luminophore. Electrolytic medium: 0.1 M  $\text{NBu}_4\text{PF}_6$ -dichloromethane.

Compounding the luminophore with ILs was also investigated. The typical IL 1-ethyl-3-methylimidazolium/bis(trifluoromethanesulfonyl)imide (EMI/TFSI) was mixed with the dye to investigate its solvent-induced gelation ability and MC response of the gel films. A solution of 11.1 g/L in a 6/1 (*v/v*) chloroform/hexane mixture showed a sol–gel transition at 40 °C and a reversible sol–gel phase transition upon heating and cooling. The electrochemical response was evaluated using the experimental set-up shown in Figure 10a. Figure 10b shows the absorption spectra and color changes when a voltage of  $-2$  V was applied to the poly (sodium 4-styrene sulfonate) side of the anode. The absorption at 450 nm decreased, and the color of the entire cell became lighter. The color did not change when the cathode and anode were switched. Compared to the data reported in a previous paper [18], the maximum absorption wavelength is shorter than that of non-quaternized oligothiophene. Therefore, the luminophores may have been decomposed, as well as cleavage of the  $\pi$ -conjugated structure by the reduction potential, resulting in an irreversible electrical response. However, the compound complexed with the ILs showed a low intensity, and no friability response was observed in the spin-coated thin films.

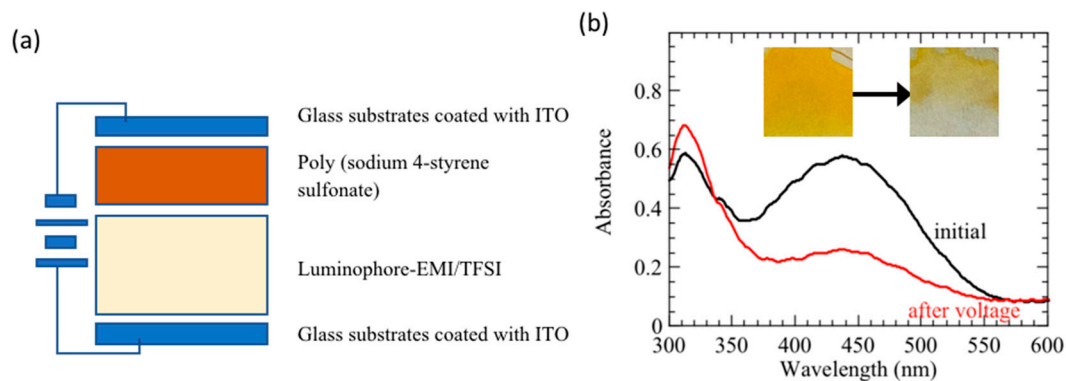


**Figure 10.** (a) Schematic of the experimental setup and (b) change in absorption spectrum of the luminophore dissolved in EMI/TFSI. The insets in (b) are photographs of the sample before (top) and after (bottom) applying  $-2$  V for 3 min.

To improve the mechanical strength of the composite, a ternary composite of polymer, IL, and dye was investigated. Shea et al. previously reported that an IL of an imidazole derivative mixed with polymethylmethacrylate (PMMA) in a 1:1 weight ratio forms a flexible and conductive gel-like composite that can be used as an electrode [24]. The 1:1 mixture of EMI/TFSI and PMMA and the luminophore showed gelation in a 1/6 (*v/v*) chloroform/hexane mixture and reversible sol–gel phase transition upon heating and cooling at 40 °C; both sol–gels showed orange luminescence under UV light irradiation. The composite solution was cast onto a glass substrate, and its response to grinding was evaluated. Figure 11a shows the changes in the PL spectrum before and after grinding. Before grinding, the powder exhibited a PL band at 637 nm, which shifted to 654 nm after grinding.

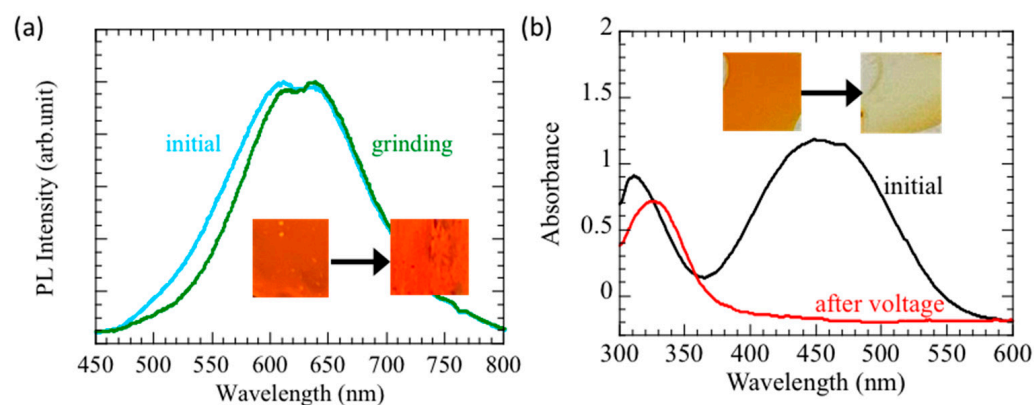
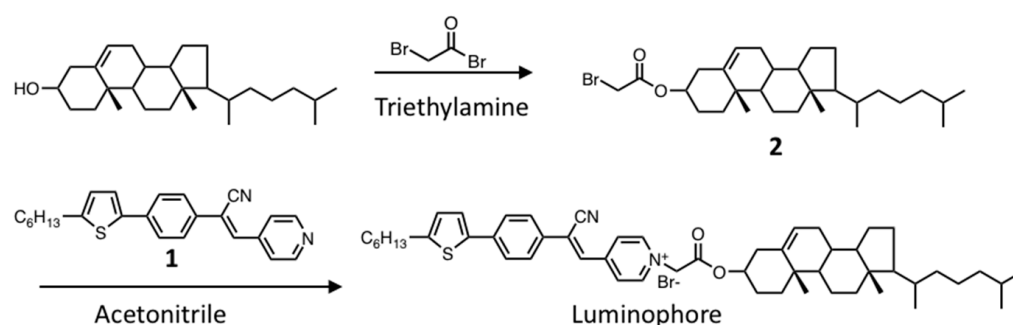


**Figure 11.** Change in (a) the PL spectrum upon mechanical grinding and (b) the absorption spectrum upon applying  $-3$  V for 3 min of the luminophore-EMI/TFSI-polymer composite. The inset in (a,b) are photographs of the composite under UV light and ambient light, respectively.

Furthermore, the electrical response was examined using the experimental system shown in Figure 11b. An irreversible color change was observed in the polymer-incorporated composite, as well as in the IL composite. Therefore, a system that can respond to both electric and abrasive stimuli was successfully constructed by combining polymers and ILs.

### 3. Materials and Methods

The synthesis of the luminophore used in this study is shown in Scheme 1. NMR and IR spectra for each compound are provided in the Supporting Information.



**Scheme 1.** Synthesis of the luminophore.

#### 3.1. Synthesis

##### 3.1.1. Synthesis of 1

Compound 1 was synthesized according to a previously reported procedure [25].

$^1\text{H}$  NMR (400 MHz,  $\text{CDCl}_3$ ),  $\delta$  (ppm): 0.91 (d,  $J = 7.5$  Hz, 3H), 1.34–1.23 (m, 6H), 1.75–1.67 (m, 2H), 2.90–2.78 (m, 2H), 6.79 (d,  $J = 3.7$  Hz, 1H), 7.26 (s, 2H), 7.47 (s, 1H), 7.66–7.62 (m, 2H), 7.68 (s, 1H), 7.75–7.71 (m, 2H), 8.77 (d,  $J = 15.3, 6.2$  Hz, 2H).

FT-IR (KBr),  $\nu$  ( $\text{cm}^{-1}$ ): 3063, 2923, 2852, 2227, 1592, 1513, 1468, 1420, and 1002.

### 3.1.2. Synthesis of 2

Cholesterol (3.82 g, 9.85 mmol) and triethylamine (8 mL) were dissolved in 20 mL THF in a 200 mL Erlenmeyer flask of Bromoacetyl bromide (2.1 g, 10.8 mmol) dissolved in 10 mL. THF was added dropwise to the reaction solution, and the reaction was stirred at room temperature for 3 h. After completion of the reaction, the by-products were removed by suction filtration, washed with THF, and the filtrate was collected. After reducing the filtrate under reduced pressure, the organic layer was washed with aqueous acetic acid and extracted with ethyl acetate. After dehydration with sodium sulfate, the filtrate was reduced under reduced pressure, purified by silica gel column chromatography, and recrystallized from THF/methanol to afford a yellow solid (1.79 g, M.p. 152 °C, 36% yield).

$^1\text{H}$  NMR (400 MHz,  $\text{CDCl}_3$ ):  $\delta$  (ppm) 8.27 (d,  $J = 8.2$  Hz, 2H), 8.02 (d,  $J = 8.2$  Hz, 2H), 7.75 (d,  $J = 7.8$  Hz, 2H), 7.70 (d,  $J = 8.2$  Hz, 2H), 7.61 (d,  $J = 11.0$  Hz, 3H), 7.47 (d,  $J = 7.8$  Hz, 2H), 7.38 (d,  $J = 8.7$  Hz, 2H), 7.20 (d,  $J = 7.8$  Hz, 2H), 2.67 (q,  $J = 7.6$  Hz, 2H), and 1.15–1.33 (3H).

IR (KBr,  $\text{cm}^{-1}$ ): 2936, 1747, 1464, 1404, 1382, 1366, 1287, 1175, and 1026.

### 3.1.3. Synthesis of the Luminophore

0.16 g (0.4 mmol) of **1** and 0.31 g (0.06 mmol) of **2** were dissolved in 50 mL acetonitrile in a 200 mL round flask and stirred in an oil bath at 80 °C for 28 h. After the completion of the reaction, the filtrate was collected by suction filtration and washed with hexane to obtain a brown solid (0.08 g M.p. 150 °C, 21% yield).

$^1\text{H}$  NMR (400 MHz,  $\text{CDCl}_3$ ),  $\delta$  (ppm): 0.71–1.66 (m, 5H), 1.13–0.85 (m, 41H), 1.29–1.38 (6H), 2.80–2.90 (2H), 3.81 (s, 2H), 6.09 (d,  $J = 5.5$  Hz, 1H), 6.79 (d,  $J = 3.7$  Hz, 1H), 7.66 (d,  $J = 8.2$  Hz, 2H), 7.85 (d,  $J = 8.7$  Hz, 2H), 8.04 (s, 1H), 8.59 (d,  $J = 6.9$  Hz, 2H), 9.25 (d,  $J = 6.9$  Hz, 2H).

$^{13}\text{C}$  NMR (101 MHz,  $\text{CDCl}_3$ ):  $\delta$  (ppm) 140.8, 121.8, 77.1, 76.8, 71.9, 56.8, 56.2, 50.2, 42.4, 39.8, 39.6, 37.3, 36.6, 36.3, 35.9, 32.0, 31.7, 31.7, 28.3, 28.1, 24.4, 23.9, 22.9, 22.7, 21.2, 18.8, and 11.9

FT-IR (KBr),  $\nu$  ( $\text{cm}^{-1}$ ): 3444, 2933, 1748, 1638, 1588, 1466, 1376, 1222, 1194, and 1056.

## 3.2. Equipment

The synthesized compounds were characterized using Fourier-transform nuclear magnetic resonance (FT-NMR; JEOL, Tokyo, Japan; JNM-ECZ 400 MHz) and infrared (FT-IR; JASCO, Tokyo, Japan; FT-IR 6000) spectroscopies.  $^1\text{H}$  and  $^{13}\text{C}$  NMR spectra were recorded for  $\text{CDCl}_3$  at room temperature using tetramethylsilane (TMS;  $\delta$  0.00) as an internal standard. Polarized light microscopy (POM; Olympus, Tokyo, Japan; BH50) and differential scanning calorimetry (DSC; Hitachi High technologies, Tokyo, Japan; DSC7020) were used to evaluate the mesomorphic properties. PL spectra were collected using an emission spectrometer (Ocean Optics, Orlando, FL, US; USB2000+) equipped with a 365 nm UV LED as the excitation source (Ocean Optics, Orlando, US; LLS-LED). The solid-state quantum yields of the luminescent materials were measured using a fluorescence spectrometer (JASCO, Tokyo, Japan; FP-6600) equipped with an integrating sphere and excited at 360 nm. The PL lifetimes of the composite films were measured using a nanosecond spectrofluorometer (Horiba, Kyoto, Japan; FluoroCube) at an excitation wavelength of 370 nm. XRD measurements were performed using a diffractometer (Rigaku, Tokyo, Japan; SmartLab 3 kW) with a standard collimated beam setup. Microscopic images of xerogels were obtained using SEM (Keyence, Osaka, Japan; V8800). Thin layers for spectroscopy and XRD were prepared by spin-casting dioxane solutions onto glass substrates. Thin layers of the luminophores or polymer composites were ground in a pen, and the luminophore powder was ground in an agate mortar. DFT calculations were performed using Gaussian16 [26] at the B3LYP/6-31+G(d) level of theory. The absorption spectra were simulated using TD-DFT at the CAM-B3LYP/6-31+G(d) level of theory. The simulated absorption spectra were calculated for the first 10 excited states using the optimized ground-state geometry as

the input geometry [27]. Cyclic voltammetry was performed using a voltammetry electrochemical analyzer (BAS, Tokyo, Japan; CV-50W) and a three-electrode cell with a carbon working electrode, a Pt counter electrode, and a  $\text{Ag}^+/\text{Ag}$  reference electrode. An  $\text{NBu}_4\text{PF}_6$  solution (0.10 M) in DCM was used as the supporting electrolyte. All the potentials were calibrated using a ferrocene  $\text{Fc}^+/\text{Fc}$  couple as an internal reference. Polymer complexes were prepared using PMMA (182230-500G, Mw: 120,000 Da,  $T_g$ : 90 °C) purchased from Sigma-Aldrich without purification. The ILs and other solvents were purchased from TCI and used without further purification.

#### 4. Conclusions

A luminescent dye with a quaternized pyridine terminus extended with cholesterol was synthesized, and its friability and electrical responsivity were evaluated. The dye exhibited a liquid crystalline phase at temperatures above 230 °C, and in the solid state, the maximum emission wavelength changed from orange emission at 637 nm to red emission at 654 nm. In complexation with EMI/TFSI, the film was gelatinized using chloroform/hexane as an auxiliary solvent; however, the deposited substrate was mechanically fragile and the MC response could not be confirmed. The dye was dissolved in a conductive gel composite of an IL and PMMA, and found that the dye exhibited a reversible sol–gel transition upon heating and cooling, forming a stable gel at room temperature. When the gel was deposited on a substrate and subjected to grinding, the emission wavelength changed from an orange-light emission wavelength of 611 nm to a red-light emission wavelength of 639 nm. Furthermore, when the gel was sandwiched between indium tin oxide electrodes and a reducing voltage of 3 V was applied, the coloration of the solution faded and, at the same time, the absorption at ~450 nm decreased, which is thought to be due to the desorption of cholesterol moieties by reduction.

Because the mechanisms of color change by electricity and luminescence color change by crushing are considered to be independent, a wider range of color changes can be expected when force and electricity are applied simultaneously. A material that can respond to electrical and mechanical stimuli can provide an intelligent skin that not only detects damage and overloads in flexible devices, but also conducts a certain amount of electricity and alerts the user to overvoltage points, such as those caused by short circuits. However, electro-responsiveness is irreversible with respect to thermoresponsiveness, and gels cannot be formed using ILs alone; these are issues that need to be addressed. In addition, as luminescent materials containing cyanostilbene are expected to change their liquid crystallinity [28] and emission color via photoreaction [29], the development of dyes that can respond to more stimuli is expected, and we plan to study these in the future.

**Supplementary Materials:** The following supporting information can be downloaded at: <https://www.mdpi.com/article/10.3390/cryst13050786/s1>, Figure S1:  $^1\text{H}$  NMR Spectrum of the **1**; Figure S2: IR spectrum of **1**; Figure S3:  $^1\text{H}$  NMR Spectrum of the **2**; Figure S4: IR spectrum of **2**; Figure S5:  $^1\text{H}$  NMR Spectrum of the luminophore; Figure S6: IR spectrum of the luminophore; Figure S7:  $^{13}\text{C}$  NMR Spectrum of the luminophore;.

**Author Contributions:** Conceptualization, N.K. and M.K.; methodology, M.K. and T.K.; software, M.K.; validation, S.Y., M.K., J.-i.N., and T.K.; investigation, S.Y. and S.S.; resources, N.K. and J.-i.N.; writing—original draft preparation, M.K.; writing—review and editing, N.K.; visualization, M.K.; supervision, N.K. All authors have read and agreed to the published version of the manuscript.

**Funding:** This study received no external funding.

**Data Availability Statement:** Data available in a publicly accessible repository.

**Conflicts of Interest:** The authors declare no conflict of interest.

## References

1. Sagiri, S.S.; Behera, B.; Rafanan, R.R.; Bhattacharya, C.; Pal, K.; Banerjee, I.; Rousseau, D. Organogels as matrices for controlled drug delivery: A review on the current state. *Soft Mater.* **2014**, *12*, 47–72. [[CrossRef](#)]
2. Yu, X.; Chen, L.; Zhang, M.; Yi, T. Low-molecular-mass gels responding to ultrasound and mechanical stress: Towards self-healing materials. *Chem. Soc. Rev.* **2014**, *43*, 5346–5371. [[CrossRef](#)] [[PubMed](#)]
3. Chen, H.; Zhou, L.; Shi, X.; Hu, J.; Guo, J.; Albouy, P.A.; Li, M.H. AIE fluorescent gelators with thermo-, Mechano-, and Vapochromic properties. *Chem. Asian J.* **2019**, *14*, 781–788. [[CrossRef](#)]
4. Agarwal, D.S.; Prakash Singh, R.P.; Jha, P.N.; Sakhuja, R. Fabrication of deoxycholic acid tethered  $\alpha$ -cyanostilbenes as smart low molecular weight gelators and AIEE probes for bio-imaging. *Steroids* **2020**, *160*, 108659. [[CrossRef](#)] [[PubMed](#)]
5. Cametti, M.; Džolić, Z. AIE-active supramolecular gel systems. In *Aggregation-Induced Emission (AIE): A Practical Guide*; Materials Today; Elsevier: Amsterdam, The Netherlands, 2022; pp. 117–164. [[CrossRef](#)]
6. Gao, A.; Wang, Q.; Wu, H.; Zhao, J.W.; Cao, X. Research progress on AIE cyanostilbene-based self-assembly gels: Design, regulation and applications. *Coord. Chem. Rev.* **2022**, *471*, 214753. [[CrossRef](#)]
7. Wang, Z.; Nie, J.; Qin, W.; Hu, Q.; Tang, B.Z. Gelation process visualized by aggregation-induced emission fluorogens. *Nat. Commun.* **2016**, *7*, 12033. [[CrossRef](#)]
8. Ku, K.; Hisano, K.; Yuasa, K.; Shigeyama, T.; Akamatsu, N.; Shishido, A.; Tsutsumi, O. Effect of Crosslinkers on Optical and Mechanical Behavior of Chiral Nematic Liquid Crystal Elastomers. *Molecules* **2021**, *26*, 6193. [[CrossRef](#)]
9. Stinson, V.P.; Shuchi, N.; McLamb, M.; Boreman, G.D.; Hofmann, T. Mechanical Control of the Optical Bandgap in One-Dimensional Photonic Crystals. *Micromachines* **2022**, *13*, 2248. [[CrossRef](#)]
10. van Esch, J.H.; Feringa, B.L. New functional materials based on self-assembling organogels: From serendipity towards design. *Angew. Chem. Int. Ed.* **2000**, *39*, 2263–2266. [[CrossRef](#)]
11. Seki, A.; Yoshio, M. Multi-color photoluminescence based on mechanically and thermally induced liquid-crystalline phase transitions of a hydrogen-bonded benzodithiophene derivative. *ChemPhysChem* **2020**, *21*, 328–334. [[CrossRef](#)] [[PubMed](#)]
12. Sagara, Y.; Kato, T. Brightly tricolored mechanochromic luminescence from a single-luminophore liquid crystal: Reversible writing and erasing of images. *Angew. Chem. Int. Ed. Engl.* **2011**, *50*, 9128–9132. [[CrossRef](#)] [[PubMed](#)]
13. Yamane, S.; Sagara, Y.; Mutai, T.; Araki, K.; Kato, T. Mechanochromic luminescent liquid crystals based on a bianthryl moiety. *J. Mater. Chem. C* **2013**, *1*, 2648–2656. [[CrossRef](#)]
14. Yagai, S.; Okamura, S.; Nakano, Y.; Yamauchi, M.; Kishikawa, K.; Karatsu, T.; Kitamura, A.; Ueno, A.; Kuzuhara, D.; Yamada, H.; et al. Design amphiphilic dipolar p-systems for stimuli-responsive luminescent materials using metastable states. *Nat. Commun.* **2014**, *5*, 4013. [[CrossRef](#)]
15. Sha, J.; Lu, H.; Zhou, M.; Xia, G.; Fang, Y.; Zhang, G.; Qiu, L.; Yang, J.; Ding, Y. Highly polarized luminescence from an AIEE-active luminescent liquid crystalline film. *Org. Electron.* **2017**, *50*, 177–183. [[CrossRef](#)]
16. Kondo, M.; Yamoto, T.; Tada, M.; Kawatsuki, N. Mechanoresponsive behavior of rod-like liquid crystalline luminophores on an alignment layer. *Chem. Lett.* **2021**, *50*, 812–815. [[CrossRef](#)]
17. Panthai, S.; Fukuhara, R.; Hisano, K.; Tsutsumi, O. Stimuli-sensitive aggregation-induced emission of organogelators containing mesogenic Au(I) complexes. *Crystals* **2020**, *10*, 388. [[CrossRef](#)]
18. Kondo, M.; Morita, Y.; Kawatsuki, N. Directional blue-shifting Mechanofluorochromic luminescent behavior of liquid crystalline composite polymeric films. *Crystals* **2021**, *11*, 000950. [[CrossRef](#)]
19. Barbee, M.H.; Mondal, K.; Deng, J.Z.; Bharambe, V.; Neumann, T.V.; Adams, J.J.; Boechler, N.; Dickey, M.D.; Craig, S.L. Mechanochromic stretchable electronics. *ACS Appl. Mater. Interfaces* **2018**, *10*, 29918–29924. [[CrossRef](#)]
20. Sum, N.; Su, K.; Zhou, Z.; Wang, D.; Fery, A.; Lissel, F.; Zhao, X.; Chen, C. “Colorless-to-Black” Electrochromic and AIE-Active Polyamides: An Effective Strategy for the Highest-Contrast Electrofluorochromism. *Macromolecules* **2020**, *53*, 10117–10127. [[CrossRef](#)]
21. Moon, H.C.; Kim, C.-H.; Lodge, T.P.; Frisbie, D. Multicolored, Low-Power, Flexible Electrochromic Devices Based on Ion Gels. *ACS Appl. Mater. Interfaces* **2016**, *8*, 6252–6260. [[CrossRef](#)] [[PubMed](#)]
22. Moon, H.C.; Lodge, T.P.; Frisbie, C.D. Solution Processable, Electrochromic Ion Gels for Sub-1 V, Flexible Displays on Plastic. *Chem. Mater.* **2015**, *27*, 1420–1425. [[CrossRef](#)]
23. Zhang, Y.; Guo, M.; Li, G.; Chen, X.; Liu, Z.; Shao, J.; Huang, Y.; He, G. Ultrastable Viologen Ionic Liquids-Based Ionogels for Visible Strain Sensor Integrated with Electrochromism, Electrofluorochromism, and Strain Sensing. *CCS Chem. In press.* [[CrossRef](#)]
24. Ji, X.; Rosset, S.; Shea, H.R. Soft tunable diffractive optics with multifunctional transparent electrodes enabling integrated actuation. *Appl. Phys. Lett.* **2016**, *109*, 191901. [[CrossRef](#)]
25. Kondo, M.; Okumoto, K.; Miura, S.; Nakanishi, T.; Nishida, J.; Kawase, T.; Kawatsuki, M. Multicolor change in the photoluminescence induced by mechanical and chemical stimuli. *Chem. Lett.* **2017**, *46*, 1188–1190. [[CrossRef](#)]
26. Frish, M.J.; Trucks, G.W.; Schlegel, H.B.; Scuseria, G.E.; Robb, M.A.; Cheeseman, J.R.; Scalmani, G.; Barone, V.; Mennucci, B.; Petersson, G.A.; et al. *Gaussian16, Revision B.01*; Gaussian, Incorp.: Wallingford, CT, USA, 2016.
27. Shkoor, M.; Mehanna, H.; Shabana, A.; Farhat, T.; Bani-Yaseen, A.D. Experimental and DFT/TD-DFT computational investigations of the solvent effect on the spectral properties of nitro substituted pyridino [3,4-c] coumarins. *J. Mol. Liq.* **2020**, *313*, 113509. [[CrossRef](#)]

28. Liu, Z.; Liao, J.; He, L.; Gui, Q.; Yuan, Y.; Zhang, H. Preparation, photo-induced deformation behavior and application of hydrogen-bonded crosslinked liquid crystalline elastomers based on  $\alpha$ -cyanostilbene. *Polym. Chem.* **2020**, *11*, 6047–6055. [[CrossRef](#)]
29. Ma, T.; Chen, S.; Du, X.; Mo, M.; Cheng, X. High-contrast fluorescence modulation driven by intramolecular photocyclization and protonation of bithienylpyridine functionalized  $\alpha$ -cyanostilbene. *Dye. Pigment.* **2023**, *213*, 111176. [[CrossRef](#)]

**Disclaimer/Publisher's Note:** The statements, opinions and data contained in all publications are solely those of the individual author(s) and contributor(s) and not of MDPI and/or the editor(s). MDPI and/or the editor(s) disclaim responsibility for any injury to people or property resulting from any ideas, methods, instructions or products referred to in the content.